Talanta 124 (2014) 43–51

Contents lists available at ScienceDirect

Talanta

journal homepage: www.elsevier.com/locate/talanta

Highly selective amperometric sensor for the trace level detection of hydrazine at bismuth nanoparticles decorated graphene nanosheets modified electrode

Rajkumar Devasenathipathy, Veerappan Mani, Shen-Ming Chen *

Department of Chemical Engineering and Biotechnology, National Taipei University of Technology, No. 1, Section 3, Chung-Hsiao East Road, Taipei 106, Taiwan, ROC

ARTICLE INFO

Article history:
Received 21 December 2013
Received in revised form
13 February 2014
Accepted 14 February 2014
Available online 20 February 2014

Keywords:
Graphene
Bismuth nanoparticles
Hydrazine
Nanomolar detection
High selectivity
Practicality

ABSTRACT

A highly selective amperometric sensor was developed for the trace level determination of hydrazine at bismuth nanoparticles (Bi) decorated graphene nanosheets (GR) composite film modified glassy carbon electrode (GCE). GR–Bi nanocomposite has been successfully prepared via simple and facile chemical reduction approach and its structure was characterized by various techniques. Surface morphological and X-ray diffraction studies revealed the formation and high loading of Bi nanoparticles on graphene sheets. GR–Bi nanocomposite modified GCE exhibited greatly enhanced electrocatalytic performance towards electro-oxidation of hydrazine in terms of decrease in overpotential and increase in oxidation peak current (I_p). The kinetic parameters such as electron transfer coefficient (α) and diffusion coefficient (D_o) of the hydrazine oxidation were determined to be 0.70 and 2.65×10^{-5} cm^2 s^{-1}, respectively. An amperometric sensor has been fabricated which detects trace level concentration of hydrazine. The sensor exhibited a wide linear range from 20 nM to 0.28 mM and a very low detection limit (LOD) of 5 nM. Remarkably, this is the lowest LOD achieved for the determination of hydrazine in neutral pH among other reported electrochemical hydrazine sensors. In addition, the sensor selectively detects hydrazine even in the presence of 1000 fold excess quantity of common interferrants. The practical feasibility of the sensor has been assessed in water and urine samples with good recoveries. Furthermore, the sensor exhibited appreciable stability, repeatability and reproducibility results.

© 2014 Elsevier B.V. All rights reserved.

1. Introduction

Hydrazine and its derivatives are well known for their widespread industrial and pharmaceutical applications such as corrosion inhibitors, plastic blowing agents, oxygen scavengers, rocket propellant, explosives, herbicides, photographic chemicals and catalysts [1–3]. Despite their extensive applications, they are highly toxic and their exposure to human beings causes severe adverse health effects [4,5]. Notably, they are classified as group B2 human carcinogens by World Health Organization (WHO) and United States Environmental Protection Agency (USEPA) [6] and hence their sensitive determination is incredibly important. Therefore several analytical methods such as titrimetry [7], spectrophotometric methods [8], flow injection analysis [9], gas chromatography–mass spectrometry (GC–MS) [10], high-performance liquid chromatography (HPLC) [11] and potentiometry [12] have been developed for the determination of hydrazine; however, most of these methods involve tedious protocols and time-consuming procedures. On the contrary, electrochemical methods are simple with rapid response and offer high sensitivity, selectivity and reliability [13]. However, electrochemical determination at conventional bare electrodes suffers from serious drawbacks such as high overpotential and electrode surface fouling related problems. These limitations can be addressed by employing chemically modified electrodes such as benzofuran–carbon nanotubes (CNTs)/ionic liquid (IL) [2], luteolin electrodeposited multi-walled carbon nanotubes (MWCNTs) and IL composite [14], quinizarine modified TiO_2 nanoparticles [15], carbon@ZnO nanorod array [16], zinc oxide nanonail [17], curcumin-MWCNTs [18], quinizarine [19], graphene [20] and cobalt nanoflowers/graphene [21] films modified electrodes. Though several modified electrodes have been reported for the electrochemical determination of hydrazine, only very few are able to detect trace level quantity of hydrazine [14,15].

* Corresponding author. Tel.: +886 2270 17147; fax: +886 2270 25238.
E-mail address: smchen78@ms15.hinet.net (S.-M. Chen).

http://dx.doi.org/10.1016/j.talanta.2014.02.031
0039-9140 © 2014 Elsevier B.V. All rights reserved.

Metal nanoparticles are well known for their interesting optical, electronic and electrocatalytic properties and consequently they find potential applications in electrochemical sensor and biosensor applications [22,23]. However, metal nanoparticles alone are not stable on the bare electrodes and hence a suitable mat is required to anchor them and harvest their excellent properties. In the past decades, significant efforts have been made to explore carbon nanotubes as supporting mats to anchor metal nanoparticles [24,25]. Recently, graphene (GR), a 2D nanomaterial composed of a flat monolayer of carbon atoms, has proved to be one of the most desired materials ascribed to its interesting physicochemical properties [26]. Notably, GR nanosheets have large surface area compared to CNTs and therefore GR can be a promising carbonaceous support material to stabilize vast amounts of metal nanoparticles. Graphene oxide (GO), an oxygenated derivative of graphene, is the ideal precursor for the preparation of graphene–metal nanoparticles composites owing to its unique advantages such as inexpensive and simple production from graphite, easy processing in aqueous dispersions and available sites for functionalization [27,28]. Remarkably, the electronic properties of GR can be easily tailored by metal nanoparticles upon composite formation and the resulting nanocomposites have shown excellent synergy between graphene and metal nanoparticles [29,30].

In the literature, metal nanoparticles such as gold (Au), palladium (Pd), rhodium (Rh), silver (Ag), platinum (Pt) and cobalt (Co) have been extensively studied as electrocatalysts for the oxidation of hydrazine [21,31–35]. Some of the reported metal nanoparticles-based hydrazine sensors include Au nanoparticle/single walled carbon nanotubes (SWCNTs) [31], bimetallic Au–Pd nanoparticles on GR nanoplates [32], Rh nanoparticles loaded carbon nanofibers [33], Ag nanoparticle on functionalized MWCNTs [34], CNTs supported Pt nanoparticles [35] and Co nanoflowers on GR [21]. However, no attempt was made in the literature to explore Bi nanoparticles for the electrochemical determination of hydrazine. Nevertheless, bismuth nanoparticles (Bi), a semi-metal known for its excellent physicochemical properties, find widespread applications in pharmaceutical and metallurgical additives [36]. Its biocompatibility, low toxicity and promising electrochemical ability make it an alternative feasible electrode material for mercury electrodes [37,38].

In the present work, we prepared graphene–bismuth nanoparticles composite (GR–Bi nanocomposite) by a simple chemical reduction approach and employed it for the sensitive determination of hydrazine. We achieved the lowest detection limit (LOD) of 5 nM for the determination of hydrazine. To the best of our knowledge, this is the lowest LOD achieved among all the electrochemical sensors available in the literature.

2. Experimental

2.1. Reagents and apparatus

Bismuth (III) nitrate pentahydrate, $Bi(NO_3)_2 \cdot 5H_2O$ was purchased from Wako pure chemical industries, Ltd. Graphite (powder, <20 μm), hydrazine and all other chemicals were purchased from Sigma-Aldrich. All the chemicals used were of analytical grade and used without further purification. 0.05 M of phosphate buffer solution (PBS) was prepared using Na_2HPO_4 and NaH_2PO_4. Double distilled water with conductivity ≥ 18 MΩ was used for all the experiments. A stock solution of hydrazine was prepared in PBS (pH 7).

Electrochemical measurements were carried out using CHI 611A work station in a conventional three-electrode cell with modified GCE as a working electrode (area 0.071 cm^2), saturated Ag|AgCl (saturated KCl) as a reference electrode and Pt wire as a counter electrode. All the electrochemical experiments were carried out at ambient temperature. Amperometric measurements were performed with analytical rotator AFMSRX (PINE instruments, USA) and rotating disc glassy carbon electrode (RDE, area 0.21 cm^2). Scanning electron microscope (SEM) and Energy-dispersive X-ray (EDX) spectra were carried out using Hitachi S-3000H scanning electron microscope and HORIBA EMAX X-ACT, respectively. X-ray diffraction (XRD) studies and attenuated total reflectance-FTIR (ATR-FTIR) spectra were carried out using an XPERT-PRO diffractometer using Cu Kα radiation ($k=1.54$ Å) and a Perkin-Elmer IR spectrometer, respectively.

2.2. Preparation of graphene–Bi nanocomposite modified electrode

The schematic representation for the preparation of graphene–Bi nanocomposite has been given in Fig. 1. Graphite oxide was prepared by Hummer's method as reported elsewhere [39] and suspended in DMF (1 mg mL^{-1}). It was exfoliated to graphene oxide (GO) via ultrasonication for 2 h. The unexfoliated graphite oxide and unoxidized graphite were removed by performing centrifugation at 3500 rpm for 20 min. The yellowish brown colored homogenous dispersion of GO was collected and used further for the preparation of GR–Bi nanocomposite. $Bi(NO_3)_2 \cdot 5H_2O$ was added to the as-prepared GO dispersion (w/w: 2:3) and ultrasonicated for 1 h. Subsequently, 0.5 ml of hydrazine monohydrate (32.1 mmol) was added and refluxed at 160 °C under nitrogen atmosphere for 24 h. Upon completion of reduction, the obtained GR–Bi nanocomposite was isolated via filtration, and washed with copious amount of water and ethanol. Finally the composite was dried overnight at 60 °C and re-dispersed in DMF (1 mg mL^{-1}).

GCE surface was polished with 0.05 μm alumina slurry using a Buehler polishing kit, cleaned and dried. Then 6 μl of graphene–Bi nanocomposite (GR–Bi nanocomposite) was drop casted onto the pre-cleaned GCE, dried at ambient conditions and used for electrochemical experiments. As a control, graphene modified GCE (graphene/GCE) was also prepared.

3. Results and discussions

3.1. Characterization of GR–Bi nanocomposite

SEM technique was employed to analyze the surface morphology of GR and GR–Bi nanocomposite. SEM image of GR (Fig. 2A)

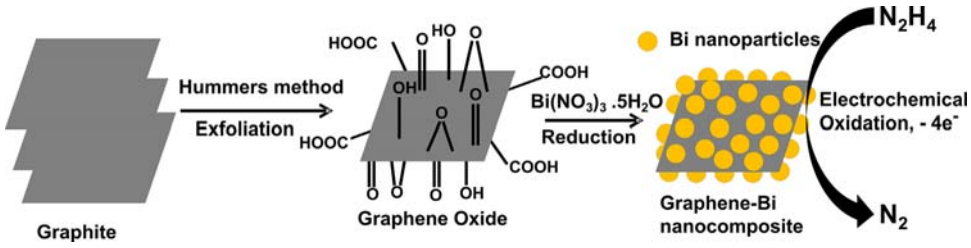

Fig. 1. Schematic representation for the preparation of GR–Bi nanocomposite.

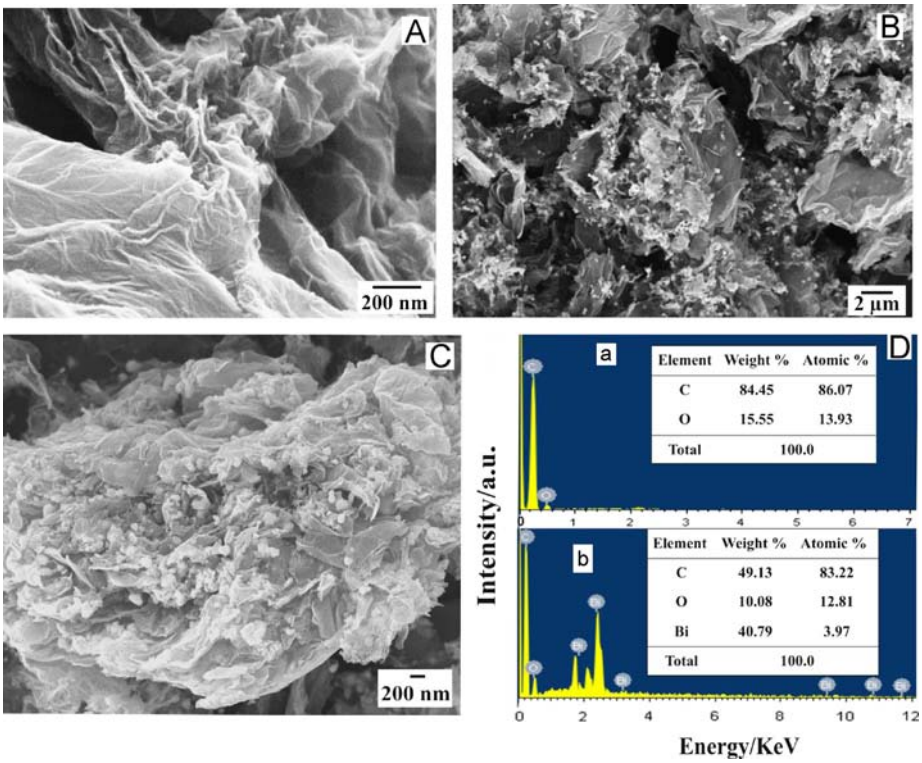

Fig. 2. SEM images of GR (A) and GR–Bi nanocomposite (B and C). (D) EDX spectra of GR (a) and GR–Bi nanocomposite (b).

depicts a typical wrinkled and scrolled intrinsic thin sheet like GR morphology. SEM image of GR–Bi nanocomposite (Fig. 2B) shows the uniform distribution of Bi nanoparticles on the sheets of the GR surface. SEM image (Fig. 2C) at low magnification shows the regular decoration and incorporation of Bi nanoparticles (size varies in the range of 50–120 nm) into thin GR sheets (thickness varies between 2 and 3 nm). EDX spectrum of GR (curve a, Fig. 2D) exhibited signals for C and O with wt% of 84.45 and 15.55, respectively, whereas EDX of GR–Bi nanocomposite (curve b, Fig. 2D) exhibited signals for C, O and Bi with wt% of 49.13, 10.08 and 40.79, respectively. The observation of 40.79 wt% of Bi revealed a high loading of Bi nanoparticles into graphene sheets. The decrease in oxygen content indicates the ample reduction of GO.

XRD pattern of GR (curve a, Fig. 3A) exhibited a broad peak centered at 2θ of 23.1°, corresponding to the graphitic network of GR. However, it was extensively broadened in the range of 20–30° in the XRD pattern of GR–Bi nanocomposite (curve b, Fig. 3A), attributed to the efficient inhibition of restacking of graphene sheets in the nanocomposite due to the presence of Bi nanoparticles. Moreover, the XRD pattern of GR–Bi nanocomposite is quite consistent with the literature XRD pattern of rhombohedral Bi nanoparticle (JCPDS no. 05-0519) [40]. ATR-FTIR spectra of GO (curve a, Fig. 3B) displays well-defined peaks, ν(–OH)=3390, ν(C=O)=1740, ν(C=C)=1626, ν(C–O, epoxy)=1243 and ν(R–O, alkoxy)=1066 cm^{-1} ascribed to the stretching vibrations of functional groups of GO. However, the fact that no peaks were observed in the AT-FTIR spectrum of GR–Bi nanocomposite (curve b, Fig. 3B) revealed the abundant reduction of oxygen functionalities.

Electrochemical behaviors of GR (curve a) and GR–Bi nanocomposite (curve b) have been investigated by cyclic voltammetry in PBS (pH 7) at the scan rate (ν) of 50 mV s^{-1} (Fig. 4). No obvious peaks were observed in the CV of the GR/GCE, whereas three notable voltammetric peaks were observed in the CV of GR–Bi nanocomposite. (1) Two anodic peaks (I and II) at the potential of −0.21 and −0.07 V related to the anodic conversion of Bi^0/Bi^+ and Bi^+/Bi^{3+}, respectively. (2) A large cathodic peak (III) appeared

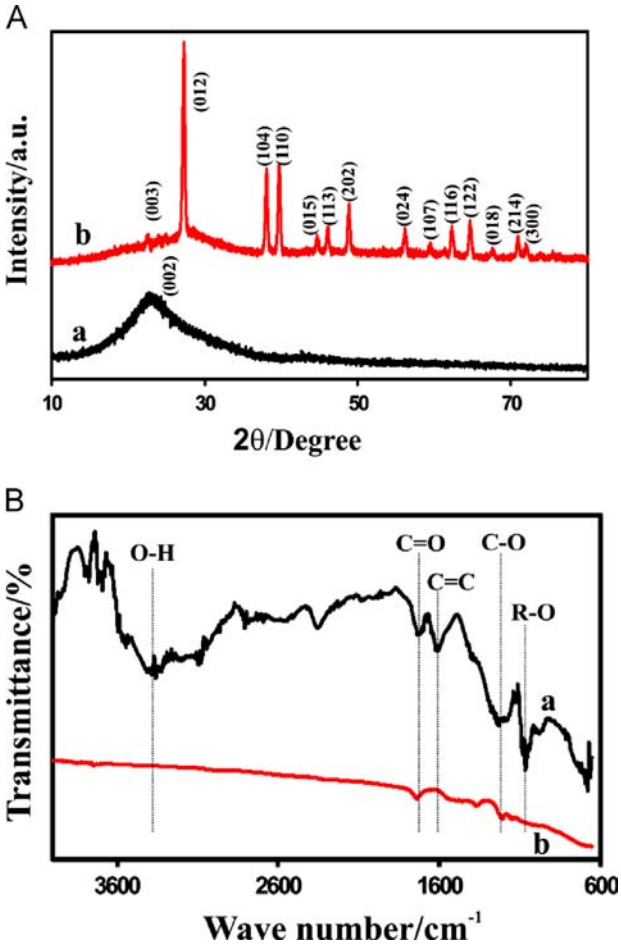

Fig. 3. (A) XRD patterns of GR (a) and GR–Bi nanocomposite (b). (B) AT-FTIR spectra of GO (a) and GR–Bi nanocomposite (b).

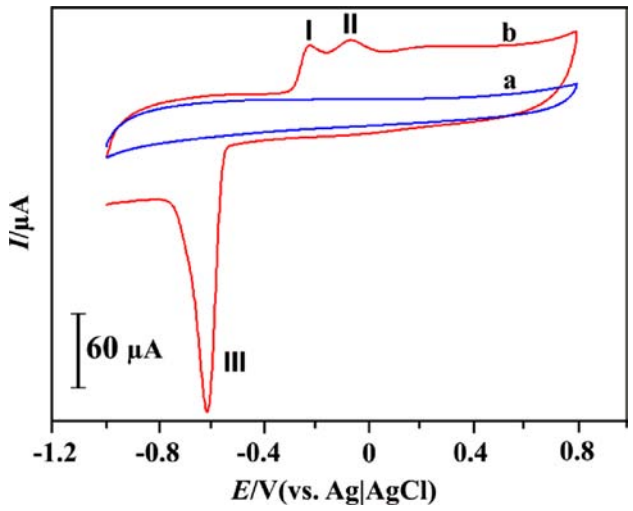

Fig. 4. (A) CVs obtained at GR/GCE (a) and GR–Bi nanocomposite (b) films modified GCEs in PBS (pH 7) at the scan rate of 50 mV s^{-1}.

at the potential of –0.62 V related to the cathodic conversion of Bi^{3+}/Bi^{0} [41]. Thus the electrochemical behavior of the Bi nanoparticles is retained in the GR–Bi nanocomposite.

3.2. Electro-oxidation of hydrazine at various modified electrodes

Fig. 5 shows the CVs of bare GCE (A), GR (B) and GR–Bi nanocomposite (C) films modified GCEs in the absence (curve a) and presence of 0.1 mM hydrazine (curve b) at the scan rate of 50 mV s^{-1}. Bare GCE exhibited very small oxidation peak at a large overpotential of +0.60 V, revealing the sluggish electrocatalytic behavior of bare GCE towards electro-oxidation of hydrazine. CV of graphene/GCE exhibited a sigmoid like curve for the oxidation of hydrazine, indicating poorly defined anodic characteristics with slow electrode kinetics. In contrast to bare GCE and GR/GCE, GR–Bi/GCE exhibited well-defined and highly enhanced oxidation peak (I_{pa}) at the potential of +0.29 V. The two peaks observed at the potential of −0.21 and −0.07 V were metal based anodic process as explained in Section 3.1. Notably the overpotential at GR–Bi/GCE is 90 mV and 360 mV lower than that at the GR/GCE and bare GCE, respectively, indicating the favorable oxidation of hydrazine at the GR–Bi/GCE. Additionally, I_p of the oxidation peak at the GR–Bi/GCE is 4.1 and 20-fold higher than that at the GR/GCE and bare GCE. The observed large decrease in overpotential and substantial increase in the oxidation peak current at the GR–Bi/GCE validated the faster electron transfer reaction of hydrazine oxidation at the GR–Bi/GCE, which in turn revealed the excellent electrocatalytic ability of the nanocomposite.

Here, the enhanced electrocatalysis is not only restricted to the electrode kinetics but also due to the semi-infinite and thin layer diffusion of hydrazine at the open pore system of GR layers [42]. Probably, Bi nanoparticles play a significant role by providing good electrocatalytic ability and able to assist in the formation of open pore system to access more hydrazine ions [43]. Furthermore, GR possesses numerous edge planes like defects which can provide additional catalytic sites to access more hydrazine ions. Moreover, there might be strong synergy between GR and Bi nanoparticles which also offered outstanding electrocatalytic ability to the nanocomposite.

The effect of pH of the supporting electrolyte has been investigated to understand the influence of various pHs towards oxidation of hydrazine. The electrocatalytic behavior of hydrazine at the GR–Bi/GCE has been studied in PBS with different pH values (pH 3–11) containing 0.1 mM hydrazine (Fig. S1). As shown in the plot, hydrazine oxidation peak current is significantly affected in different pH solutions. The oxidation peak current increased with

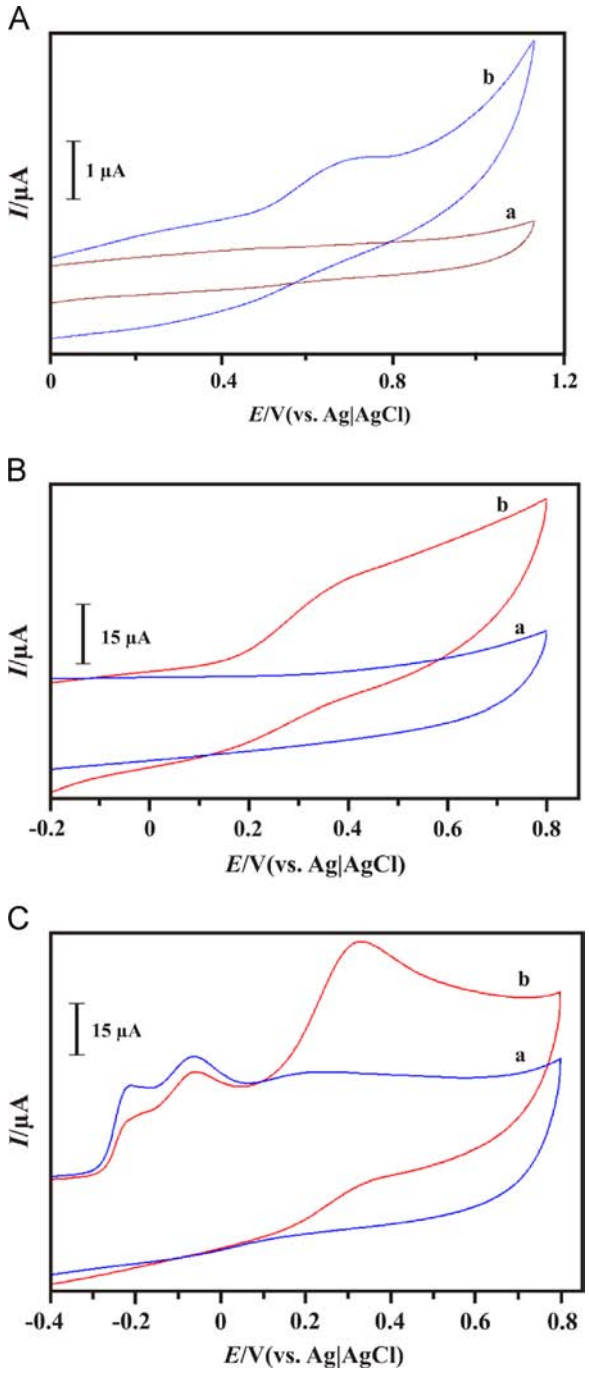

Fig. 5. CVs obtained at bare (A), GR (B) and GR–Bi nanocomposite (C) film modified GCEs in PBS (pH 7) in the absence (a) and presence of 0.1 mM hydrazine (b).

increasing pH from 3 to 7 and attained maximum at pH 7 and then persisted as constant in the basic pHs from 7 to 9. In the acidic buffer solutions, hydrazine ions might be highly protonated which is not active for the electrocatalytic oxidation. Additionally, pK_a value of the hydrazine is 7.9 and hence the peak current decreases in acidic pH between 3 and 7 [44]. Since the maximum electrocatalytic response of hydrazine at the GR–Bi/GCE was observed at pH 7, we chose this pH for all the electrochemical experiments.

3.3. Different scan rates

The effect of scan rate (ν) towards the oxidation of hydrazine (0.1 mM) at the GR–Bi/GCE was examined in PBS (pH 7) at the scan

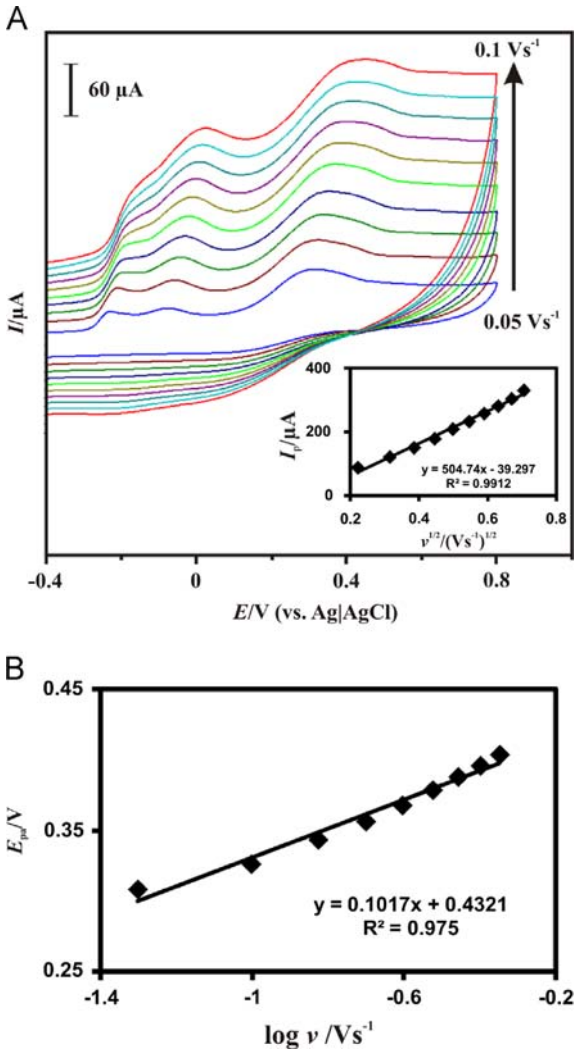

Fig. 6. (A) CVs obtained at GR–Bi/GCE in PBS (pH 7) containing 0.1 mM hydrazine at different scan rates from 0.05 V s^{-1} to 0.5 V s^{-1}. Inset: plot of $\nu^{1/2}$ vs. I_p. (B) Plot of log ν vs. I_p.

rate ranges from 0.05 to 0.5 V s^{-1} (Fig. 6A). The anodic peak current of hydrazine observed at the potential of +0.30 V increased linearly with increase in scan rates from 0.05 to 0.5 V s^{-1}. In addition, the peak potential of the anodic peak was shifted to more positive values when scan rate increased. A plot of square root of scan rates ($\nu^{1/2}$) and anodic peak current (I_p) exhibited a linear relationship, indicating that the hydrazine oxidation occurring at the GR–Bi/GCE is a diffusion controlled electron transfer process (inset of Fig. 6A). The corresponding linear regression equation can be expressed as I_p (µA)=504.74$\nu^{1/2}$ (V s^{-1})$^{1/2}$–39.297, R^2=0.9912.

A plot of E_{pa} vs. log ν presumes a linear relationship and therefore the electrocatalytic oxidation of hydrazine at the GR–Bi/GCE is an electrochemically irreversible process (Fig. 6B). The corresponding linear regression equation can be expressed as E_{pa} (V)=0.1017 log ν (V s^{-1})+0.4324. E_{pa} can be represented by Tafel by the following equation,

$$E_{pa} = [2.303RT/(1-\alpha)n_aF] \log \nu + K \quad (1)$$

where α is the electron transfer coefficient, n_a is the number of electron transfer involved in the rate-determining step, and K is the constant. The constants R, T and F have their usual meanings (R=8.314 J K^{-1} mol^{-1}, T=298 K, F=96485 C mol^{-1}). Here, the Tafel slope is 101.7 mV/decade (Fig. 5b), indicating that one electron transfer was involved in the rate determining step of the oxidation process. By substituting the value of n_a as 1 and the slope of E_{pa} versus log ν in Eq. (1), the value of α was estimated to be 0.70. Furthermore, the number of electrons (n) involved in the overall hydrazine oxidation process has been calculated from the following equation [45]:

$$I_p = (2.99 \times 10^5)n[(1-\alpha)n_a]^{1/2}AC_oD_o^{1/2}\nu^{1/2} \quad (2)$$

where D_o (cm^2 s^{-1}) is the diffusion coefficient of hydrazine (2.65×10^{-5} cm^2 s^{-1}, estimated via chronoamperometry in Section 3.4), A is the electrode area (0.071 cm^2), C_o (0.1×10^{-3} mol cm^{-3}) is the bulk concentration of hydrazine and the other parameters have their conventional meanings. By substituting all the values in the above Eq. (2), the value of n was estimated to be about 4. Consequently, the electro-oxidation of hydrazine at the GR–Bi/GCE involves four electrons and the following mechanism can be proposed for the oxidation of hydrazine, which is consistent with the literature reports [44].

$$N_2H_4 + H_2O \rightarrow N_2H_3 + H_3O^+ + e^- \text{ (slow)} \quad (3)$$

$$N_2H_3 + 3H_2O \rightarrow N_2 + 3H_3O^+ + 3e^- \text{ (fast)} \quad (4)$$

Here, the first step is the rate-determining step involving one-electron transfer (Eq. (3)) followed by the fast second step involving the three-electron transfer process (Eq. (4)). Thus, the overall hydrazine oxidation reaction involves four-electron transfer and can be summarized as the following equation,

$$N_2H_4 + 4H_2O \rightarrow N_2 + 4H_3O^+ + 4e^- \quad (5)$$

3.4. Chronoamperometry

In order to evaluate the apparent diffusion coefficient (D_0) of hydrazine at the GR–Bi/GCE, a series of chronoamperometry experiments was carried out. Fig. S2A shows the chronoamperograms obtained at the GR–Bi/GCE towards different concentrations of hydrazine: 0.1 (a), 0.5 (b), 0.9 (c), 1.3 (d), 1.7 (e), 2.1 (f) and 2.5 mM (g) in N_2 saturated PBS (pH 7). Cottrell plots were made between net electrolysis current (I/µA) versus $t^{-1/2}$/$s^{-1/2}$) for each of the concentrations (Fig. S2B). The Cottrell equation can be expressed as the following equation [46],

$$I = nFAC_0^*D^{1/2}\pi^{-1/2}t^{-1/2} \quad (6)$$

where C_0^* is the concentration of hydrazine (mol cm^{-3}) and the other parameters have their usual meanings as explained for Eq. (1). By substituting the slopes of the Cottrell plots and other parameters in Cottrell Eq. (5), the mean value of D_0 can be calculated to be 2.65×10^{-5} cm^2 s^{-1} which is comparable to the value reported by the previous reports [47].

3.5. Determination of hydrazine:CV and LSV

Fig. 7A shows the CVs obtained at GR–Bi/GCE in the absence (curve a) and presence of hydrazine concentration ranging from 0.2 to 2.6 mM (curves b–n; each addition of 0.2 mM) in PBS (pH 7). The potential range is applied between –0.3 V and 0.8 V and the scan rate is held at 50 mV s^{-1}. Upon the addition of 0.2 mM hydrazine into the PBS solution, a sharp and obvious peak is observed at the potential of +0.30 V, attributed to the electro-oxidation of hydrazine. The peak current increased linearly upon further additions of hydrazine. The linear increase in the oxidation peak current shows the occurrence of efficient electrocatalytic ability of the modified electrode. A plot of peak current versus concentration of hydrazine exhibited a linear relationship (inset of Fig. 7A). The respective linear regression equation can be expressed as I_p (µA)=115.04 [hydrazine] (mM)+65.03, R^2=0.986. The linear concentration range is observed from 0.1 to

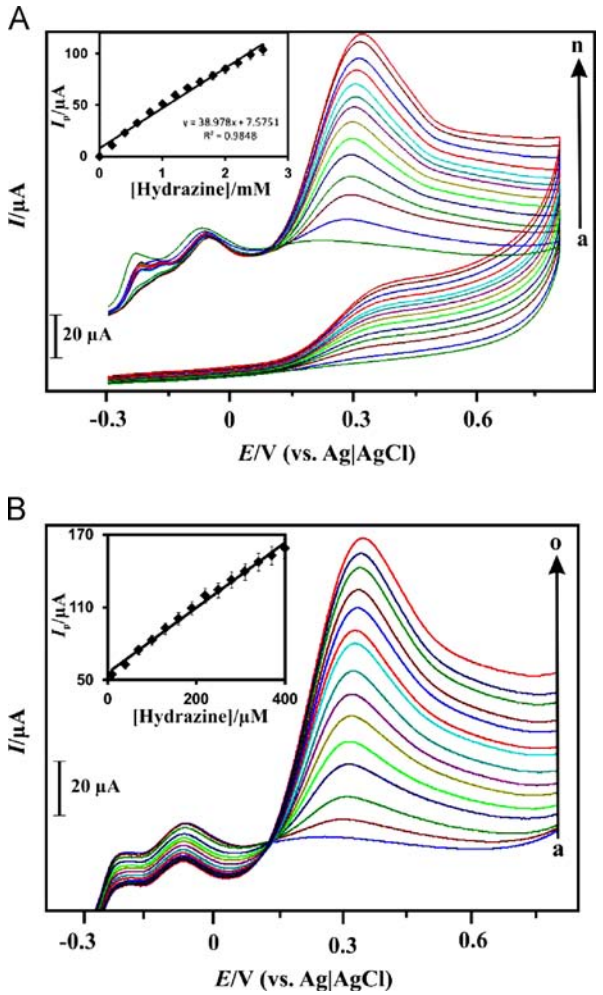

Fig. 7. (A) CVs obtained at GR–Bi/GCE in the absence (a) and presence of 0.2–2.6 mM hydrazine (curves b–n; each addition of 20 mM) in PBS (pH 7) at the scan rate 50 mV s^{-1}. Inset: plot of [Hydrazine] vs. I_p. (B) LSVs obtained at GR–Bi/GCE in the absence (a) and presence of 10–400 μm hydrazine (curves b–o; each addition of 30 μm) in PBS (pH 7) at the scan rate 50 mV s^{-1}. Inset: plot of [hydrazine] vs. I_p.

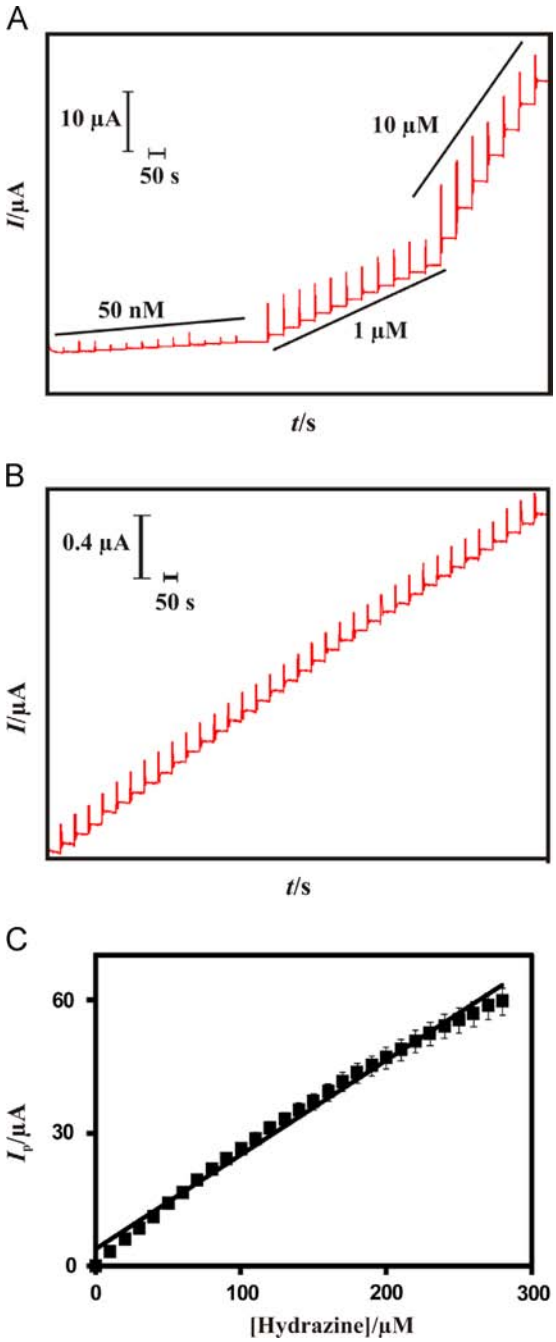

Fig. 8. (A) Amperometric *i–t* response of GR–Bi nanocomposite film modified rotating disc GCE upon each addition of 50 nM (a), 1 μM (b) and 10 μM (c) hydrazine into continuously stirred PBS (pH 7) at the rotation speed of 1500 rpm. E_{app} = +0.30 V. (B) Amperometric *i–t* response of GR–Bi nanocomposite film modified rotating disc GCE upon each addition of 50 nM hydrazine into continuously stirred PBS (pH 7). (C) Plot of [Hydrazine] vs. I_p.

2.6 mM and the sensitivity is 115.04 μA mM^{-1}. This must be attributed to the excellent electrocatalytic ability of the GR–Bi/GCE towards oxidation of hydrazine without any fouling effect.

Linear sweep voltammograms (LSV) were recorded at GR–Bi/GCE in the absence (curve a; each addition of 30 μM and presence of 10–400 μM (curves b–o; each addition of 30 μM) of hydrazine in PBS (pH 7) (Fig. 7B). A sharp anodic peak was observed at +0.30 V upon 10 μM addition of hydrazine and the peak current increases linearly upon further increase in hydrazine concentration (curves b–o). A plot between concentration of hydrazine and peak currents exhibited a linear relationship and the respective linear regression equation can be expressed as I_p (μA) = 0.269 [hydrazine] (μM) + 55.668, R^2 = 0.9934 (inset of Fig. 7B). The linear concentration range varies between 10 and 400 μM and the sensitivity is 0.269 μA $μM^{-1}$.

3.6. Amperometric determination of hydrazine

Fig. 8A shows the amperometric *i–t* response of GR–Bi nanocomposite film modified rotating disc GCE upon each addition of 50 nM (a), 1 μM (b) and 10 μM (c) hydrazine into continuously stirred PBS (pH 7) at the rotation speed of 1500 rpm. Applied potential (E_{app}) of the electrode was held at +0.30 V. Fig. 8B shows the amperogram obtained at GR–Bi nanocomposite film modified rotating disc GCE for each sequential addition of 50 nM hydrazine. The sensor exhibited quick and sensitive amperometric response towards each addition of hydrazine. The amperometric response current reaches its 95% steady-state current within 5 s, indicating the fast electrocatalytic oxidation of hydrazine at the GR–Bi/GCE. A calibration plot was made between the concentration of hydrazine versus response current (Fig. 8C) and the respective linear regression equation can be expressed as I_p (μA) = 0.3134 [hydrazine] (μM) + 3.616. The response current for each addition increases linearly as the concentration of hydrazine increases over the linear range between 20 nM and 280 μM. The sensitivity of the sensor was estimated to be 1.492 μA $μM^{-1}$ cm^{-2} from the slope of

Table 1
Comparison of analytical parameters for the hydrazine determination at GR–Bi nanocomposite film modified GCE with other films modified electrodes.

Electrode	Method	α[a]	D_0 ($cm^2\ s^{-1}$)[b]	LOD[c] (μM)	LR[d] (μM)	Ref.
Benzofuran-CNT/ionic liquid composite	DPV[e]	0.55	$(1.1 \pm 0.1) \times 10^{-5}$	0.066	0.1–40, 0.1–600	[3]
Luteolin/MWNT-ionic liquid composite	Amperometry	0.61	NA[f]	0.0066 (6.6 nM)	0.02–0.2, 0.2–120	[14]
Quinizarine/TiO_2 nanoparticles	DPV	0.5	1.93×10^{-5}	0.077	0.5–1900	[15]
C@ZnO nanorod array	Amperometry	NA	NA	0.1	0.1–3.8	[16]
ZnO nanonails	Amperometry	NA	NA	0.2	0.1–1.2	[17]
Curcumin/MWCNTs	Amperometry	0.55	2.45×10^{-6}	1.4	2–44	[18]
Quinizarine	DPV	0.35	1.1×10^{-6}	0.14	0.2–1.0, 2.0–10	[19]
Graphene	Amperometry	NA	NA	1	3–300	[20]
Cobalt nanoflowers/graphene	Amperometry	–	–	0.1	0.25–370, 370–2200	[21]
AuNPs/choline	LSV[g]	0.5	2.46×10^{-5}	0.1	0.5–500	[44]
AuPd/graphene	Amperometry	NA	NA	0.2	2–185	[49]
Ni(II)-baicalein complex/MWCNT	Amperometry	0.65	3.58×10^{-5}	0.8	2.5–200	[50]
PVP[h]-AgNCs	Amperometry	NA	NA	1.1	5–460	[51]
TiO_2–Pt hybrid nanofibers	Amperometry	NA	NA	0.142	0.142–1030	[52]
Overoxidized polypyrrole	Amperometry	0.64	3.1×10^{-5}	3.7	1.3–2000	[53]
GR–Bi nanocomposite	Amperometry	0.70	2.65×10^{-5}	0.005 (5 nM)	0.02–280	This work

[a] α: Electron transfer coefficient.
[b] D_0: Diffusion coefficient.
[c] LOD: Detection limit.
[d] LR: Linear range.
[e] DPV: Differential pulse voltammetry.
[f] NA: Not available.
[g] LSV: Linear sweep voltammetry.
[h] PVP-AgNCs: poly(vinylpyrrolidone)-protected silver nanocubes.

the calibration plot. The limit of detection (LOD) of the sensor was calculated to be 5 nM using the formula, $LOD = 3s_b/S$ (where s_b = standard deviation of blank signal and S = sensitivity) [48]. The important parameters of the sensor, such as α, D_o, LOD and linear range of the GR-B-/GCE towards determination of hydrazine, have been compared with other modified electrodes available in the literature (Table 1). As can be seen from Table 1, the proposed sensor exhibited quite comparable performance with other sensors. Notably, the achieved LOD of 5 nm is the lowest LOD achieved among all the other modified electrodes. This must be ascribed to the outstanding electrocatalytic ability of the GR–Bi/GCE for the sensitive determination of hydrazine.

In order to further explore the role of Bi nanoparticles towards sensitive detection of hydrazine, amperometry experiments were carried out in the absence (GR only, curve a) and presence of Bi nanoparticles (GR–Bi/GCE, curve b) upon successive addition of 50 nM hydrazine into continuously stirred PBS (pH 7) (Fig. S3). No noteworthy amperometric responses were observed in the amperogram of GR/GCE (curve a), whereas quick and stable responses were observed in the amperogram of GR–Bi/GCE. Thus, GR alone cannot detect nanomolar concentration of hydrazine which is also consistent with the previous report [20], whereas its unique assembly with Bi nanoparticles can offer nanomolar detection with greatly enhanced electrocatalytic performance. This shows the special role of Bi nanoparticles towards the exceptional electrocatalytic ability of the GR/Bi nanocomposite for the trace level detection with high sensitivity.

3.7. Selectivity studies

Selectivity of the proposed sensor towards hydrazine determination was investigated in the presence of a variety of likely interferences such as common ions and biological interferrants (Fig. 9). GR–Bi/GCE exhibited well-defined response towards each 100 nM hydrazine (a), whereas no noteworthy responses were observed for the 1000-fold excess concentration of F^- (b), Cl^- (c), Br^- (d), I^- (e), CO_3^{2-} (f), NO_3^-(g), NO_2^- (h), $(COO)_2^{2-}$ (i), Na^+ (j), Mg^{2+} (k), Ca^{2+} (l), Ba^{2+} (m), Fe^{2+} (n), Co^{2+} (o), Ni^{2+}(p), Zn^{2+} (q), NH_4^+ (r), glucose (s), fructose (t), L-Arginine (u) and 200-fold of ascorbic acid (v). However, an immediate response was observed upon addition of 100 nM hydrazine into the aforementioned interferences coexisted electrolyte solution. Hence, GR–Bi/GCE has excellent selectivity towards the sensitive determination of hydrazine even in the presence of 1000-fold large quantities of common ions and biological interferrants.

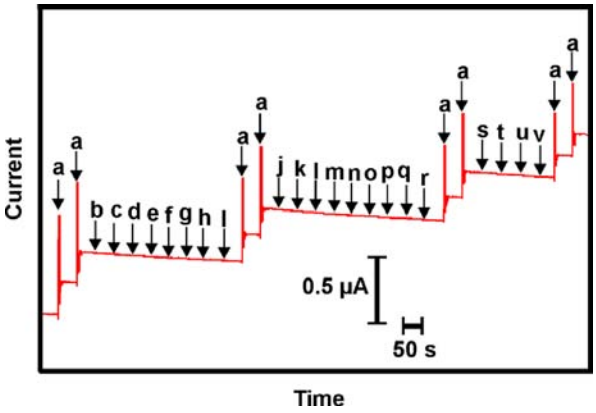

Fig. 9. Amperometric response of GR–Bi nanocomposite film modified rotating disc GCE for the 100 nM addition of hydrazine (a) in the presence of 1000-fold excess concentration of F^- (b), Cl^- (c), Br^- (d), I^- (e), CO_3^{2-} (f), NO_3^- (g), NO_2^- (h), $(COO)_2^{2-}$ (i), Na^+ (j), Mg^{2+} (k), Ca^{2+} (l), Ba^{2+} (m), Fe^{2+} (n), Co^{2+} (o), Ni^{2+}(p), Zn^{2+} (q), NH_4^+ (r), glucose (s), fructose (t), L-Arginine (u) and 200-fold excess concentration of ascorbic acid (v).

3.8. Determination of hydrazine in real samples

In order to evaluate the practicality of the sensor towards determination of hydrazine, water samples collected from tap and rain water were employed (Table 2). The spiked hydrazine concentrations were of 100 and 300 nM. The determined concentrations are: rain water (102.6 and 302.1 nM) and tap water (98.39 and 297.3 nM). The corresponding recoveries are: rain water (102.6% and 100.7%) and tap water (98.39% and 99.11%).

Table 2
Determination of hydrazine in water and urine samples at the GR–Bi nanocomposite film modified GCE.

Samples	Added (μM)	Found (μM)	Recovery (%)	RSD[a] (%)
Rain water	100	102.6	102.6	3.3
	300	302.1	100.7	3.8
Tap water	100	97.85	97.85	2.8
	300	297.4	99.14	3.1
Urine sample	100	98.41	98.41	3.5
	300	296.8	98.93	3.9

[a] Relative Standard Deviation of 3 individual measurements.

In addition, human urine sample was also employed to study the practical feasibility of the sensor. The spiked hydrazine concentrations were of 100 and 300 nM. The determined concentrations are 98.41 and 296.8 nM and the corresponding recoveries were 98.41% and 98.93%, respectively. Appreciable recoveries achieved in the determination of hydrazine in various water samples and human urine samples revealed the practical feasibility of the sensor towards trace level detection of hydrazine.

3.9. Repeatability, reproducibility and stability studies

Repeatability and reproducibility of the proposed GR–Bi/GCE based sensor have been evaluated using CV studies in N_2 saturated PBS containing 0.1 mM hydrazine at the scan rate of 50 mV s^{-1}. The sensor presented appreciable repeatability with relative standard deviation (R.S.D) of 2.18% for 10 repetitive measurements carried out using single electrode. In addition, the sensor presented acceptable reproducibility of 2.93% for the six independent measurements carried out in six different electrodes.

In order to determine the storage stability of the modified electrode, the electrocatalytic response of the GR–Bi/GCE towards 0.1 mM of hydrazine was monitored every day. The electrode was stored in PBS (pH 7) at 4 °C when not in use. During the one-month storage period, the sensor exhibited well-defined catalytic response towards hydrazine detection without any shift in the peak potential. Remarkably, 93.45% of the initial I_p was retained over one month of continuous use, revealing the good storage stability of the sensor. The stability of the GR–Bi nanocomposite film modified electrode under hydrodynamic conditions is mandatory for the amperometric sensing applications. Therefore, we attempt to study the operational stability of GR–Bi/GCE in the presence of 100 nM hydrazine. The GR–Bi/GCE was rotated continuously at 1500 rpm ($E_{app} = +0.30$ V). Stable amperometric response was observed and only 8.7% of the initial response current was decreased even after being continuously rotated for 3000 s, indicating the excellent operational stability of the modified electrode.

4. Conclusions

In summary, we successfully prepared GR–Bi nanocomposite by a simple and facile chemical method and characterized by SEM, EDX, XRD, AT-FTIR and CV techniques. Graphene–Bi/GCE exhibited superior electrocatalytic ability towards the oxidation of hydrazine. The developed amperometric sensor exhibited excellent analytical parameters such as wide linear range from 20 nM to 0.28 mM, low LOD (5 nM) and high sensitivity (1.492 μA μM^{-1} cm^{-2}) for the determination of hydrazine. Moreover, the sensors possess high selectivity towards the determination of hydrazine even in the presence of 1000-fold excess quantity of common interferents. The practical feasibility of the sensor towards the determination of a nanomolar quantity of hydrazine was assessed in water and urine samples with good recoveries. The sensor exhibited acceptable stability, repeatability and reproducibility. The outstanding electrocatalytic ability, good stability, fast response, high selectivity and sensitivity of the proposed sensor revealed that graphene–Bi NPs composite can be explored as a promising electrode material for the other electrochemical sensor applications.

Acknowledgment

This work was supported by the National Science Council and the Ministry of Education of Taiwan (Republic of China).

Appendix A. Supplementary material

Supplementary data associated with this article can be found in the online version at http://dx.doi.org/10.1016/j.talanta.2014.02.031.

References

[1] J.E. Troyan, Eng. Chem. Res. 45 (1953) 2608–2612.
[2] Y. Wang, Y. Wan, D. Zhang, Electrochem. Commun. 12 (2010) 187–190.
[3] M.M. Ardakani, A. Khoshroo, Electrochim. Acta 103 (2013) 77–84.
[4] E.H. Vernot, J.D. MacEwen, R.H. Bruner, C.C. Haun, E.R. Kinkead, D.E. Prentice, A. Hall , R.E. Schmidt, R.L. Eason, G.B. Hubbard, J.T. Young, Fundam. Appl. Toxicol. 5 (1985) 1050–1064.
[5] D. Steinhoff, U. Mohr, J. Exp. Pathol. 33 (1988) 133–143.
[6] World Health Organization, Environmental Health Criteria 68: Hydrazine, Geneva, Switzerland, 1987, pp. 1–89.
[7] P.V.K. Rao, G.G. Rao, Talanta 20 (1973) 907–910.
[8] F. Dias, A.S. Olojola, B. Jaselskis, Talanta 26 (1979) 47–49.
[9] S. Ikeda, H. Satake, Y. Kohri, Chem. Lett. 13 (1984) 873–876.
[10] M. Sun, L. Bai, D.Q. Liu, J. Pharm. Biomed. Anal. 49 (2009) 529–533.
[11] C.M. Morenoa, T. Stadler, A.A. Silva, L.C.A. Barbosa, M.E.L.R. Queiroz, Talanta 89 (2012) 369–376.
[12] M.A. Koupparis, T.P. Hadjiioannou, Talanta 25 (1978) 477–480.
[13] S.K. Kim, Y.N. Jeong, M.S. Ahmed, J.-M. You, H.C. Choi, S. Jeon, Sens. Actuators B 153 (2011) 246–251.
[14] S.-H. Wu, F.-H. Nie, Q.-Z. Chen, J.-J. Sun, Anal. Methods 2 (2010) 1729–1736.
[15] M.M. Ardakani, Z. Taleat, H. Beitollahia, H. Naeimi, Nanoscale 3 (2011) 1683–1689.
[16] J. Liu, Y. Li, J. Jiang, X. Huang, Dalton Trans. 39 (2010) 8693–8697.
[17] A. Umar, M.M. Rahman, S.H. Kim, Y.-B. Hahn, Chem. Commun. (2008) 166–168.
[18] L. Zheng, J.-F. Song, Sens. Actuators B 135 (2009) 650–655.
[19] M.M. Ardakani, P.E. Karami, P. Rahimi, H.R. Zare, H. Naeimi, Electrochim. Acta 52 (2007) 6118–6124.
[20] C. Wang, L. Zhang, Z. Guo, J. Xu, H. Wang, K. Zhai, X. Zhuo, Microchim. Acta 169 (2010) 1–6.
[21] Y. He, J. Zheng, S. Dong, Analyst 137 (2012) 4841–4848.
[22] C.N.R. Rao, G.U. Kulkarni, P.J. Thomas, P.P. Edwards, Chem. Soc. Rev. 29 (2000) 27–35.
[23] A.A. Lazarides, K.L. Kelly, T.R. Jensen, G.C. Schatz, J. Mol. Struct.: THEOCHEM 529 (2000) 59–63.
[24] B. Wu, Y. Kuang, X. Zhang, J. Chen, Nano Today 6 (2011) 75–90.
[25] R. Muszynski, B. Seger, P.V. Kamat, J. Phys. Chem. C 112 (2008) 5263–5266.
[26] V. Singh, D. Joung, L. Zhai, S. Das, S.I. Khondaker, S. Seal, Prog. Mater. Sci. 56 (2011) 1178–1271.
[27] D.R. Dreyer, S. Park, C.W. Bielawski, R.S. Ruoff, Chem. Soc. Rev. 39 (2010) 228–240.
[28] D. Chen, H. Feng, J. Li, Chem. Rev. 112 (2012) 6027–6053.
[29] C. Xu, X. Wang, J. Zhu, J. Phys. Chem. C 112 (2008) 19841–19845.
[30] Q. Zhuo, Y. Ma, J. Gao, P. Zhang, Y. Xia, Y. Tian, X. Sun, J. Zhong, X. Sun, Inorg. Chem. 52 (2013) 3141–3147.
[31] P.V. Dudin, P.R. Unwin, J.V. Macpherson, Phys. Chem. Chem. Phys. 13 (2011) 17146–17152.
[32] Q. Wan, Y. Liu, Z. Wang, W. Wei, B. Li, J. Zou, N. Yang, Electrochem. Commun. 29 (2013) 29–32.
[33] G. Hua, Z. Zhou, Y. Guo, H. Hou, S. Shao, Electrochem. Commun. 12 (2010) 422–426.
[34] G. Gao, D. Guo, C. Wang, H. Li, Electrochem. Commun. 9 (2007) 1582–1586.
[35] S. Chakraborty, C.R. Raj, Sens. Actuators B 147 (2010) 222–227.
[36] M. Yarema, M.V. Kovalenko, G. Hesser, D.V. Talapin, W. Heiss, J. Am. Chem. Soc. 132 (2010) 15158–15159.
[37] C.N. Tharamani, H.C. Thejaswini, S. Sampath, Bull. Mater. Sci. 31 (2008) 207–212.
[38] Y. Luo, C. Wang, Y. Qiao, M. Hossain, L. Ma, M. Su, J. Mater. Sci. – Mater. Med. 23 (2012) 2563–2573.
[39] W.S. Hummers, R.E. Offeman, J. Am. Chem. Soc. 80 (1958) 1339.

[40] P.K. Sahoo, B. Panigrahy, S. Sahoo, A.K. Satpati, D. Li, D. Bahadur, Biosens. Bioelectron. 43 (2013) 293–296.
[41] M. Yang, Z. Hu, J. Electroanal. Chem. 583 (2005) 46–55.
[42] I. Streeter, G.G. Wildgoose, L. Shao, R.G. Compton, Sens. Actuators B: Chem. 133 (2008) 462–466.
[43] W. Lv, D.-M. Tang, Y.-B. He, C.-H. You, Z.-Q. Shi, X.-C. Chen, C.-M. Chen, P.-X. Hou, C. Liu, Q.-H. Yang, Nano Lett. 3 (2009) 3730–3736.
[44] J. Li, H. Xie, L. Chen, Sens. Actuators B 153 (2011) 239–245.
[45] C.-Y. Lin, A. Balamurugan, Y.-H. Lai, K.-C. Ho, Talanta 82 (2010) 1905–1911.
[46] S. Thiagarajan, R.F. Yang, S.-M. Chen, Int. J. Electrochem. Sci. 6 (2011) 4537–4552.
[47] M.M. Ardakani, H. Rajabi, B.B.F. Mirjalili, H. Beitollahi, A. Akbari, J. Solid State Electrochem. 14 (2010) 2285–2292.
[48] A. Radoi, D. Compagnone, E. Devic, G. Palleschi, Sens. Actuators B 121 (2007) 501–506.
[49] Y. Liu, B. Li, W. Wei, Q. Wan, N. Yang, Adv. Mater. Res. 704 (2013) 246–251.
[50] L. Zheng, J.-F. Song, Talanta 79 (2009) 319–326.
[51] Y. Wang, X. Yang, J. Bai, X. Jiang, G. Fan, Biosens. Bioelectron. 43 (2013) 180–185.
[52] Y. Ding, Y. Wang, L. Zhang, H. Zhang, C.M. Lic, Y. Lei, Nanoscale 3 (2011) 1149–1157.
[53] M.R. Majidi, A. Jouyban, K.A. Zeynali, Electrochim. Acta 52 (2007) 6248–6253.